ORIGINAL PAPER

Double-walled core-shell structured Si@SiO$_2$@C nanocomposite as anode for lithium-ion batteries

Hua-Chao Tao · Xue-Lin Yang · Lu-Lu Zhang · Shi-Bing Ni

Abstract Double-walled core-shell structured Si@SiO$_2$@C nanocomposite has been prepared by calcination of silicon nanoparticles in air and subsequent carbon coating. The obtained Si@SiO$_2$@C nanocomposite demonstrates a reversible specific capacity of about 786 mAh g^{-1} after 100 cycles at a current density of 100 mA g^{-1} with a capacity fading of 0.13 % per cycle. The enhanced electrochemical performance can be due to that the double walls of carbon and SiO$_2$ improve the electronic conductivity and enhance the compatibility of electrode materials and electrolyte as a result of accommodating the significant volumetric change during cycles. The interlayer SiO$_2$ may release the mechanical strain and enhance the interfacial adhesion between carbon shell and silicon core.

Keywords Li-ion batteries · Anodes · Electrochemical characterizations · Electrochemical stabilities · Charging/discharging

Introduction

With increasing energy demand, lithium-ion batteries with high energy density and long life span are strongly desired from a utility standpoint. Among various anode materials, silicon is very attractive for the next generation high-energy rechargeable lithium-ion batteries because of its highest theoretical specific capacity of 4,200 mAh G^{-1} and satisfactory potentials for lithium ion insertion and extraction [1]. In addition, the silicon as anode materials has the advantages of

H.-C. Tao · X.-L. Yang (✉) · L.-L. Zhang · S.-B. Ni
College of Materials and Chemical Engineering, Collaborative Innovation Center for Energy Equipment of Three Gorges Region, China Three Gorges University, 8 Daxue Road, Yichang, Hubei 443002, China
e-mail: xlyang@ctgu.edu.cn

abundance in nature and environmentally friendly. However, the large volume changes of Si during lithium ion insertion and extraction lead to the pulverization of the electrode materials and thus causing the decay of capacity with cycling [2, 3]. Moreover, the low electronic conductivity of Si can cause the polarization of electrode during cycling process.

To overcome these problems, many strategies have been implemented, especially focusing on reducing the silicon particle size and preparation of silicon/carbon composites. Various nanostructured silicon materials (silicon nanoparticles [4], silicon nanotubes [5], silicon hollow nanospheres [6], silicon nanowires [7], silicon nanonests [8], silicon nanoarrays [9]) exhibit improved electrochemical performance because nanosized silicon could buffer volume stress and shorten the Li-ion diffusion path lengths. In addition, silicon/carbon composites (silicon/carbon nanorods [10], silicon/carbon nanospheres [11], silicon/graphene nanosheets [12], silicon/carbon nanotubes [13], silicon/carbon nanofibers [14], silicon/graphite [15], silicon/fullerene [16]) have been widely studied to improve the cycling stability. The carbon can prevent aggregation of Si nanoparticles and improve electronic conductivity of electrode. Furthermore, carbon coating can release the mechanical stress caused by large volume changes of Si during charge/discharge process and protect the Si electrode from direct contact with the electrolyte due to the superior chemical and electrochemical stabilities of carbon, thus stabilizing the solid electrolyte interphase (SEI) layer and enhancing the cycle life of Si-based electrodes. Core-shell-structured Si/C composite can combine the advantages of silicon core (high capacity) and carbon shell (long cycle life and high electronic conductivity). Core-shell-structured Si/C nanocomposites have been prepared to obtain a stable capacity because of the homogeneous distribution of Si nanoparticles in carbon matrix [17, 18]. Core-shell-structured Si/C composites are usually formed by mixing active materials with carbon precursor and then heat treatment at high

temperature in an inert atmosphere. It is difficult to form a uniform carbon layer on the surface of active particles due to the weak interface bond between active materials and carbon coating. Su et al. report the SiO_2 layer is beneficial to coating a dense carbon layer on silicon [19].

Herein, we report a simple and large-scale method for preparation of double-walled core-shell structured $Si@SiO_2@C$ nanocomposite though calcination of silicon nanoparticles in air to obtain core-shell-structured $Si@SiO_2$ nanocomposite followed by carbon coating. The thin interlayer SiO_2 (~5 nm) can strengthen adhesion of the carbon shell and silicon core. The obtained double-walled core-shell structured $Si@SiO_2@C$ nanocomposite exhibits an excellent cycling stability.

Experimental

Preparation of $Si@SiO_2@C$ nanocomposite

The double-walled core-shell structured $Si@SiO_2@C$ nanocomposite was prepared through two steps. Firstly, 1 g of Si nanoparticles was calcined in air at 700 °C for 2 h to form a layer of SiO_2 on the surface of Si. Secondly, to prepare double core-shell-structured $Si@SiO_2@C$ nanocomposite, predetermined amount of epoxy resin as carbon source was heated to 100 °C and then the $Si@SiO_2$ nanocomposite was added into the epoxy resin until vigorous stirring to obtain a gel. The gel was calcined at 700 °C under Ar atmosphere for 1 h to get double-walled core-shell structured $Si@SiO_2@C$ nanocomposite. For comparison, $Si@C$ nanocomposite was obtained according to the above method without calcination of Si in air.

Structural characterization

X-ray diffraction patterns were collected on a Rigaku Ultima IV with filtered Cu Ka radiation. Raman spectra were recorded on LabRAM HR800 (Horiba JobinYvon) with a laser wavelength of 532 nm. Transmission electron microscope (TEM, JOEL JEM-200CX) and high-resolution TEM (HR-TEM) were employed to visualize the morphology and particle size. Thermogravimetric analysis (TGA) was carried out in air from 25 to 1,000 °C on a PerkinElmer Instruments Diamond TG/DTA.

Electrochemical measurements

The electrochemical properties were investigated by using CR2032 coin cells. The working electrodes were prepared by mixing the active materials ($Si@SiO_2@C$ nanocomposite, $Si@C$ nanocomposite, and Si nanoparticles), carbon black (Super P) and polyvinylidene difluoride (PVDF) at a weight

ratio of 80:10:10 in N-methyl-2-pyrrolidone (NMP) solvent to form slurry. The slurry was pasted on Cu foil and then dried at 120 °C for 24 h. The electrolyte was 1 M $LiPF_6$ in ethylene carbonate/dimethyl carbonate with a volume ratio of 1:1, and lithium foil was used as the counter electrode. Coin cells were fabricated in an Ar-filled glove box with the concentration of moisture and oxygen below 1 ppm. Galvanostatic discharge and charge measurements were performed at a rate of 100 mA g^{-1} between 0.01 and 1.5 V using a land CT2100 battery test system. Cyclic voltammograms (CV) were measured on a CHI660C Electrochemical Workstation (Shanghai Chenhua) with a voltage range from 0.01 to 1.5 V at a scan rate of 0.5 mV s^{-1}. Electrochemical impedance spectra (EIS) were collected from 0.01 Hz to 100 kHz with an alternating current amplitude of 5 mV using a CHI660C Electrochemical Workstation (Shanghai Chenhua).

Results and discussion

Figure 1a illustrates the schematic diagram of the fabrication procedure for $Si@SiO_2@C$ nanocomposite. The $Si@SiO_2@C$ nanocomposite was obtained by forming a SiO_2 layer on the surface of Si nanoparticles and subsequent coating a carbon layer. The $Si@SiO_2@C$ nanocomposite is spherical with a diameter in the range of 100 to 200 nm (Fig. 1b). The Si nanoparticles are well coated into SiO_2 and carbon shells, the double walls SiO_2 and carbon can encapsulate completely the Si core (Fig. 1b). The HR-TEM (Fig. 1c) image reveals that the Si nanoparticles are coated with a layer of SiO_2 and carbon layer, and the thickness of interlayer SiO_2 is about 5 nm. The coating carbon shell exhibits a disordered microstructure. No obvious SiO_2 layer is observed in $Si@C$ nanocomposite, indicating that the Si nanoparticles are directly coated with carbon layer (Fig. 1d).

The XRD patterns and Raman spectra of $Si@SiO_2@C$ nanocomposite and Si nanoparticles are presented in Fig. 2. In the case of $Si@SiO_2@C$ nanocomposite, the main diffraction peaks at 28.5, 47.4, 56.2, 69.2 76.4, and 88.1° can be indexed as the (111), (220), (311), (400), (331), and (400) planes of Si crystallites (JCPDF NO. 27–1402), respectively. No diffraction peak corresponding to SiO_2 and graphite is observed, indicating that the interfacial layer SiO_2 and carbon shell are both amorphous. The Raman spectra of Si nanoparticles and $Si@SiO_2@C$ nanocomposite are compared in Fig. 2b. For the $Si@SiO_2@C$ nanocomposite, the sharp peak at about 506 cm^{-1} is due to the Si-Si stretching mode [20]. The peaks at 1,360 and 1,582 cm^{-1} are assigned to the D band and G band of carbon, respectively [21]. Three-dimensional ratio of D band to G band is about 1.26 for $Si@SiO_2@C$ nanocomposite, indicating the presence of the disordered carbon in nanocomposite, which is consistent with the above XRD result [22].

Fig. 1 A schematic diagram of the fabrication for double-walled core-shell structured Si@SiO$_2$@C nanocomposite (**a**); TEM (**b**) and HR-TEM images (**c**) of Si@SiO$_2$@C nanocomposite; HR-TEM image of Si@C nanocomposite (**d**)
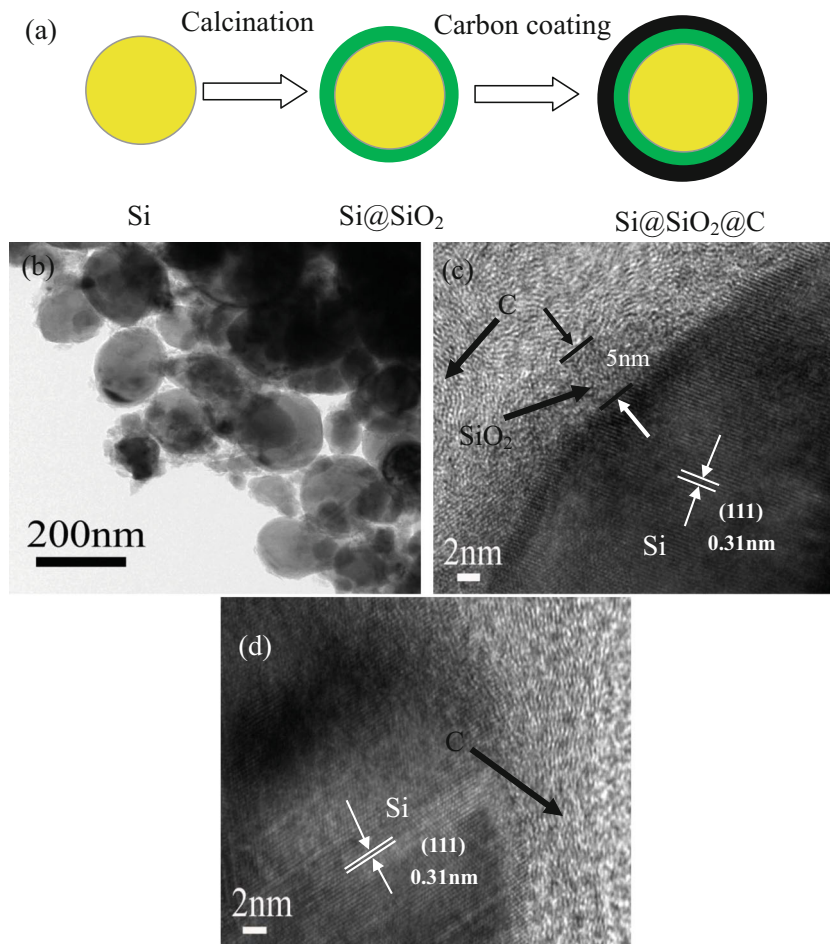
From the TGA curves of Si@SiO$_2$@C and Si@C nanocomposites (Fig. 3), it can be estimated that the weight contents of carbon in the Si@SiO$_2$@C and Si@C nanocomposites are about 57 and 55 %, respectively. The first discharge (lithium ion insertion)-charge (lithium ion extraction) curves of Si@SiO$_2$@C nanocomposite, Si@C naocomposite, and Si nanoparticles at a rate of 100 mA g^{-1} between 0.01 and 1.5 V are displayed in Fig. 4a. The cycling stabilities for Si@SiO$_2$@C nanocomposite, Si@C nanocomposite, and Si nanoparticles are presented in Fig. 4b. In case of Si@SiO$_2$@C nanocomposite, there is a discharge plateau at 0.1 V corresponding to the reaction of between lithium ions and silicon. The Si@SiO$_2$@C nanocomposite delivers the first discharge specific capacity and charge specific capacity of 1,755 and 911 mAh g^{-1} (the capacity is based on the total nanocomposite), respectively. The reversible capacity of Si@SiO$_2$@C is still as high as 845 mAh G^{-1} after 80 cycles, suggesting that the enhanced cycle stability of Si@SiO$_2$@C in comparison with Si@C nanocomposite and Si nanoparticles. After 80 cycles, the reversible capacity of Si@SiO$_2$@C starts to decrease slightly and the reversible capacity is about 785 mAh g^{-1} after 100 cycles.

A control sample of only carbon-coated Si nanoparticles without forming the interlayer SiO$_2$ shows much faster capacity decay and lower stable capacity than the one with interlayer SiO$_2$. The reversible specific capacity for Si@C nanocomposite decreases from an initial 1,057 mAh g^{-1} to less than 500 mAh g^{-1} after 65 cycles. The Si nanoparticles also fail to afford good cycling performance with continuous capacity decay over 50 cycles. These results suggest that the SiO$_2$ and carbon-coating layers on the surface of Si nanoparticles are two important factors to the observed cycling stability in the Si@SiO$_2$@C nanocomposite. The interlayer SiO$_2$ on the surface of Si nanoparticles could provide a flexible cushion in the Si@SiO$_2$@C nanocomposite to accommodate stress and volume changes. In addition, the interlayer SiO$_2$ also could enhance the adhesion between silicon core and carbon shell. Furthermore, the carbon on the Si@SiO$_2$ nanocomposite affords electrical conductivity to the Si nanoparticles. These factors all contributed to the relative excellent performance of the Si@SiO$_2$@C nanocomposite anode materials.

The electrochemical reaction mechanism of Si@SiO$_2$@C anode was clearly revealed using CV. The CV curves of Si@SiO$_2$@C electrode are plotted in Fig. 5. There are two
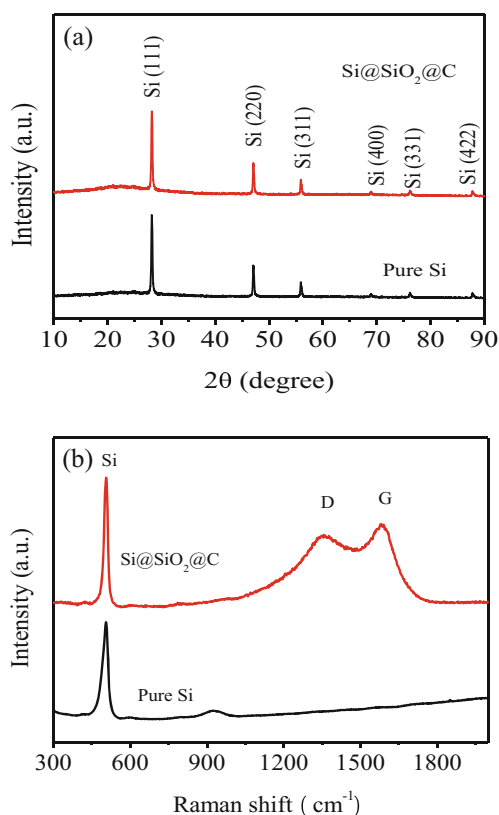
Fig. 2 X-ray diffraction patterns (a) and Raman spectra (b) for Si@SiO$_2$@C nanocomposite and Si nanoparticles

peaks at 0.66 and 0.1 V during the first lithiation process due to the formation of SEI layer and Li$_x$Si alloy, respectively. The peak at 0.66 V disappears at the subsequent cycles, suggesting the formation of stable SEI layer in the first discharge process. Two peaks at around 0.32 and 0.51 V during the delithation process are corresponding to the dealloying process of Si with lithium. These results are consistent with the above discharge–charge curves.

In order to further investigate the mechanism of the enhanced electrochemical performance, EIS measurements were performed and the obtained Nyquist plots of Si@SiO$_2$@C
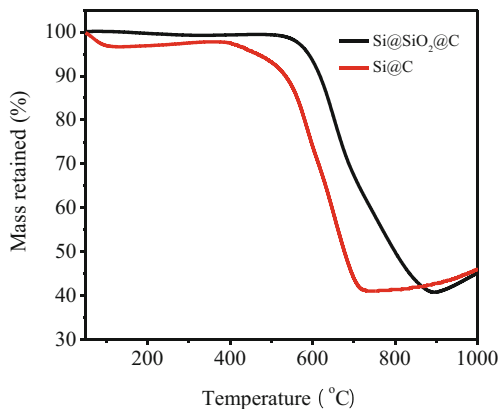

Fig. 3 TGA curves of Si@SiO$_2$@C nanocomposite and Si@C nanocomposite under air atmosphere
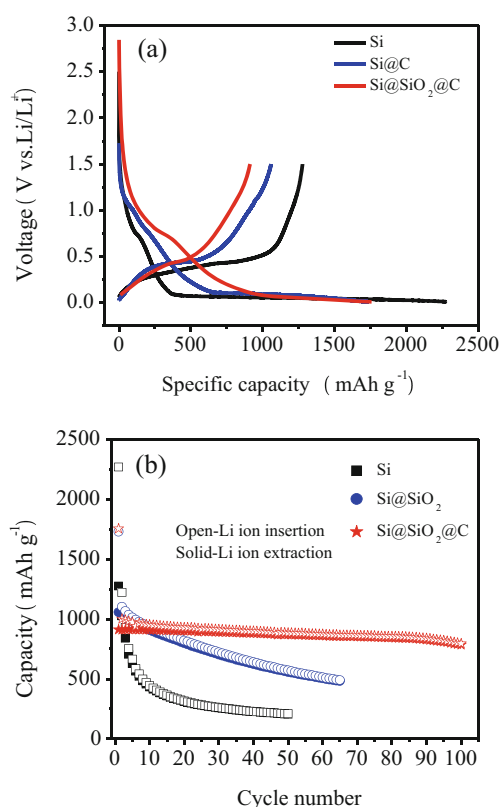

Fig. 4 The first discharge–charge curves (a) and cycling performance (b) of Si@SiO$_2$@C nanocomposite and Si nanoparticles cycled between 0.01 and 1.5 V at a rate of 100 mA g^{-1}

nanocomposite and Si nanoparticles after the first and 20th cycles are compared in Fig. 6. The plots are composed of one depressed semicircle in the high frequency range and an inclined line in the low frequency range. The depressed semi-circle in the high frequency region corresponds to the overlap between SEI film resistance and the charge transfer impedance [23], while the incline line in the low frequency region is attributed to the lithium ion diffusion within electrode [24]. The Si@SiO$_2$@C electrode exhibits the resistances with a small variance about 42Ω for the first cycle and 57Ω after 20 cycles, while the resistance of Si nanoparticles increases
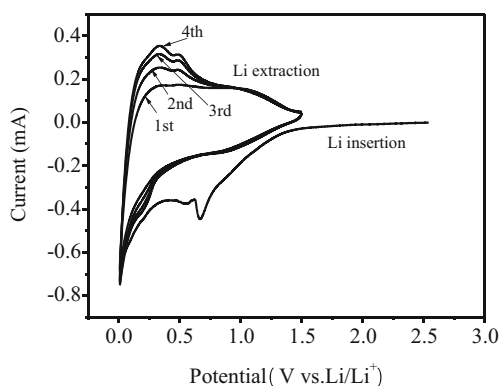

Fig. 5 Cyclic voltammetry of Si@SiO$_2$@C nanocomposite from 0.01 to 1.5 V at a scan rate of 0.5 mV s^{-1}
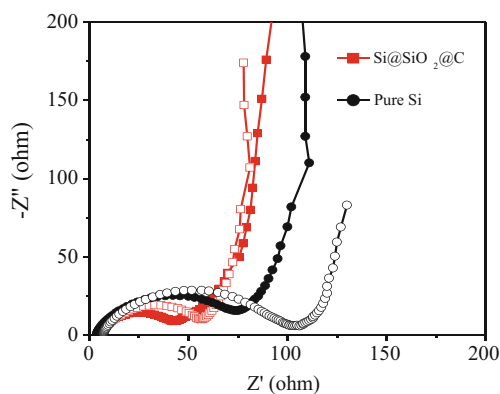
Fig. 6 Nyquist plots of Si@SiO$_2$@C nanocomposite and Si nanoparticles after the first (*solid*) and 20th (*open*) cycles, charged to 1.5 V followed by 24 h rest in an open-circuit potential

from 72 to 105 Ω after 20 cycles. The smaller interface resistance and resistance change for Si@SiO$_2$@C nanocomposite are due to the coating carbon shell, which improves the electric conductivity and enhances the compatibility of electrode and electrolyte as a result of suppressing the resistance increase.

To characterize the morphology of Si@SiO$_2$@C nanocomposite after cycling, the morphology of Si@SiO$_2$@C nanocomposite after 20 cycles was observed (Fig. 7). Although the spherical structure is not as well defined, the Si cores are still well coated by carbon, indicating the good connect between carbon and silicon. The Si@SiO$_2$@C nanocomposite improves the cycling stability of Si electrode but needs to be further studied to obtain the high capacities for hundreds of cycles.

The electrochemical reaction mechanism of SiO$_2$ with lithium ions has been studied [25], as follows:

$$SiO_2 + 4Li^+ + 4e \rightarrow Li_4SiO_4 + Si \qquad (a)$$

$$Si + xLi^+ + xe \leftrightarrow Li_xSi \qquad (b)$$

The reaction of (a) is irreversible and the reaction of (b) is reversible, and the reversible capacity of nanocomposite is determined by the reaction (b). The schematic illustration for
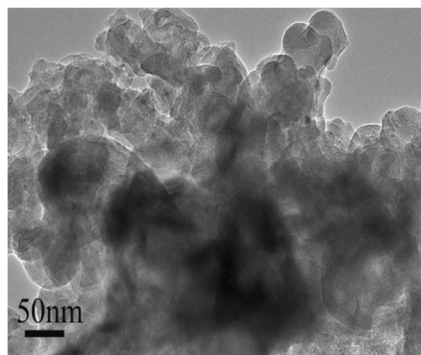

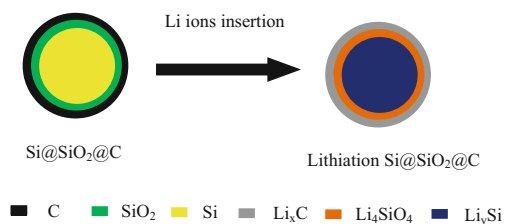Fig. 7 TEM image of Si@SiO$_2$@C nanocomposite after 20 cycles

Fig. 8 The model for lithium ion insertion into the Si@SiO$_2$@C nanocomposite

the insertion of lithium ions into the Si@SiO$_2$@C nanocomposite is displayed in Fig. 8. According to the reaction (a), the SiO$_2$ interlayer may change to the Li$_4$SiO$_4$ phase under the insertion of lithium ions. The Li$_4$SiO$_4$ phase can transfer Li ions from carbon shell to silicon core and maintain the structural integrity of electrode materials [25].

Conclusion

Double-walled core-shell structured Si@SiO$_2$@C nanocomposite was synthesized and studied as an anode material for lithium-ion batteries, and it exhibits a high storage capacity and an excellent cycling stability. The thin interlayer SiO$_2$ enhances the adhesion of carbon shell and Si core and can alleviate mechanism stress acts as inactive phase. The carbon shell also can alleviate mechanism stress caused by the large volume changes of Si and improve electronic conductivity, thus enhancing the cycling stability. The Si@SiO$_2$@C nanocomposite with high specific capacity and good cycling stability is a promising potential material for future lithium-ion batteries with high energy density.

References

1. Winter M, Besenhard JO, Spahr ME, Novak P (1998) Insertion electrode materials for rechargeable lithium batteries. Adv Mater 10:725–763
2. Huggins RA (1999) Lithium alloy negative electrodes. J Power Sources 81:13–19
3. Boukamp BA, Lesh GC, Huggins RA (1981) All-solid lithium electrodes with mixed-conductor matrix. J Electrochem Soc 128: 725–729
4. Li H, Huang XJ, Chen LQ, Wu ZG, Liang Y (1999) A high capacity nano-Si composite anode material for lithium rechargeable batteries. Electrochem Solid State Lett 2:547–549
5. Park MH, Kim MG, Joo J, Kim K, Kim J, Ahn S, Cui Y, Cho J (2009) Silicon nanotube battery anodes. Nano Lett 9:3844–3847
6. Yao Y, McDowell MT, Ryu I, Wu H, Liu N, Hu LB, Nix WD, Cui Y (2011) Interconnected silicon hollow nanospheres

for lithium-ion battery anodes with long cycle life. Nano Lett 11:2949–2954

7. Chan CK, Peng HL, Liu G, McIlwrath K, Zhang XF, Huggins RA, Cui Y (2008) High-performance lithium battery anodes using silicon nanowires. Nat Nanotechnol 3:31–35

8. Ma H, Cheng FY, Chen J, Zhao JZ, Li CS, Tao ZL, Liang J (2007) Nest-like silicon nanospheres for high-capacity lithium storage. Adv Mater 19:4067–4070

9. Song T, Xia JL, Lee JH, Lee DH, Kwon MS, Choi JM, Wu J, Doo SK, Chang H, Park W, Zang DS, Kim HS, Huang YG, Hwang KC, Rogers JA, Paik U (2010) Arrays of sealed silicon nanotubes as anodes for lithium ion batteries. Nano Lett 10:1710–1716

10. Tao HC, Fan LZ, Qu XH (2012) Facile synthesis of ordered porous Si@C nanorods as anode materials for Li-ion batteries. Electrochim Acta 71:194–200

11. Tao HC, Huang M, Fan LZ, Qu XH (2012) Interweaved Si@SiO$_x$/C nanoporous spheres as anode materials for Li-ion batteries. Solid State Ionics 220:1–6

12. Tao HC, Fan LZ, Mei YF, Qu XH (2011) Self-supporting Si/reduced graphene oxide nanocomposite films as anode for lithium ion batteries. Electrochem Commun 13:1332–1335

13. Wang W, Kumta PN (2010) Nanostructured hybrid silicon/carbon nanotube heterostructures: reversible high-capacity lithium-ion anodes. ACS Nano 4:2233–2241

14. Cui LF, Yang Y, Hsu CM, Cui Y (2009) Carbon–silicon core–shell nanowires as high capacity electrode for lithium ion batteries. Nano Lett 9:3370–3374

15. Yang XL, Wen ZY, Xu XX, Lin B, Lin ZX (2006) High-performance silicon/carbon/graphite composites as anode materials for lithium ion batteries. J Electrochem Soc 153:A1341–A1344

16. Arie AA, Song JO, Lee JK (2009) Structural and electrochemical properties of fullerene-coated silicon thin film as anode materials for lithium secondary batteries. Mater Chem Phys 113:249–254

17. Ng SH, Wang JZ, Wexler D, Konstantinov K, Guo ZP, Liu HK (2006) Highly reversible lithium storage in spheroidal carbon-coated silicon nanocomposites as anodes for lithium-ion batteries. Angew Chem Int Ed 45:6896–6899

18. Gao PF, Fu JW, Yang J, Lv RG, Wang JL, Nuli YN, Tang XZ (2009) Microporous carbon coated silicon core/shell nanocomposite via in situpolymerization for advanced Li-ion battery anode material. Phys Chem Chem Phys 11:11101–11105

19. Su L, Zhou Z, Ren M (2010) Core double-shell Si@SiO$_2$@C nano-composites as anode materials for Li-ion batteries. Chem Commun 46:2590–2592

20. Chan CK, Patel RN, O'Connell MJ, Korgel BA, Cui Y (2010) Solution-grown silicon nanowires for lithium-ion battery anodes. ACS Nano 4:1443–1450

21. Lee H, Cho J (2007) Sn$_{78}$Ge$_{22}$@carbon core–shell nanowires as fast and high-capacity lithium storage media. Nano Lett 7:2638–2641

22. Kim H, Cho J (2007) Synthesis and morphological, electrochemical characterization of Sn$_{92}$Co$_8$ nanoalloys for anode materials in Li secondary batteries. J Electrochem Soc 154:A462–A466

23. Ruffo R, Hong SS, Chan CK, Huggins RA, Cui Y (2009) Impedance analysis of silicon nanowire lithium ion battery anodes. J Phys Chem C 113:11390–11398

24. Wang C, Appleby AJ, Little FE (2001) EIS study of hydrogen insertion under restricted diffusion conditions: I. Two-step insertion reaction. J Electroanal Chem 497:3–17

25. Guo BK, Shu J, Wang ZX, Yang H, Shi LH, Liu Y, Chen LQ (2008) Electrochemical reduction of nano-SiO$_2$ in hard carbon as anode material for lithium ion batteries. Electrochem Commun 10:1876–1878